Optimization of High-quality Carbon Fiber Production from Electrospun Aligned Lignin Fibers

Jiawei Chen[1], Tanushree Ghosh[1,2], and Tian Tang[1*], and Cagri Ayranci[1*]

[1]Department of Mechanical Engineering, University of Alberta, 116 St & 85 Ave, Edmonton, Alberta, Canada
[2]Center for Earth Sciences, Indian Institute of Science, CV Raman Road, Bengaluru, Karnataka 560012, India

*Corresponding Authors: Tian Tang, Cagri ayranci

Email: tian.tang@ualberta.ca; cayranci@ualberta.ca; Tel: +1 780 492 5467 Tel: +1 780 492 2791

Abstract

In recent years, investigating lignin as an alternative carbon fiber precursor has received immense research attention as a way to reduce the cost and replace the unsustainable conventional petroleum-based precursors for carbon fiber production. The predominant challenge for lignin-based carbon fibers is its low mechanical performance compared to conventional ones. In this work, mechanical properties of electrospun lignin carbon fiber mats were shown to be considerably enhanced via alignment of the submicron fibers. Over 60% of the fibers were aligned via a rotating drum collector utilized during fiber production. The main electrospinning parameters, namely electric field, rotating speed, and flow rate were optimized with the Box-Behnken method to enhance mechanical properties with reduced fiber diameter and improved fiber alignment. The optimal electrospinning process parameter was achieved at 2000 rpm collection speed, 80 kV/m electric field, and 440 nl/s flow rate. The lignin carbon fibers produced under the optimized condition exhibited elastic modulus of 3145.47±917.75 MPa, tensile strength of 18.78±6.11 MPa, and average fiber diameter of 697.07 ± 96.41 nm. The analysis on the interactions between electrospinning parameters has laid a solid foundation for the production of high-quality carbon fibers from lignin precursor.

Keywords: electrospinning; lignin; carbon fiber; optimization; mechanical properties

Introduction

Carbon fiber (CF) is a predominant material utilized in advanced applications including tissue scaffolds[1], aerospace[2], supercapacitors[3,4], batteries[5–7], water filtration[8] and automobile industry[9] due to its high specific stiffness and strength. CF was first commercialized in the early 1960s[10]. Fibers with carbon content > 92 wt% are qualified as CF whereas those with > 99 wt% carbon are considered as graphite fibers[11]. Mechanical performance of CF ranges from low-strength (~1.0 GPa) and low-modulus (<100 GPa) for general purpose grade CF, to high-strength (>3.0 GPa) or ultrahigh-strength (>4.5 GPa) and high-modulus (350-450 GPa) or ultrahigh-modulus (>450 GPa) for high performance (HP) grade CF [12–14]. The most common CF precursors are polyacrylonitrile (PAN)[15] accounting for 90%, and pitch[16] accounting for 5% CF production around the world. PAN-based CFs manifest superior tensile performance to suffice aerospace or military grade demand, but precursor cost, accounting for over 50% of the CF cost, vastly surpasses process and labor cost[17,18]. Furthermore, PAN and pitch are synthesized from petroleum or coal[19], hence unsustainable and provoking inimical influences on environment[20]. Lignin-based carbon fiber (LBCF) is a sustainable material developed to address rising environmental issues and overexploitation of natural resources. LBCF manufacturing emerged in 1969 as an alternative to common fossil-derived CF precursors[21]. To unravel the dilemma of lowering precursor cost and retaining tensile properties, lignin was introduced as a renewable phenylpropanoid-based biopolymer with high natural abundance[22]. Lignin can be obtained by recovering from waste byproduct (black liquor) of pulp mill, hence reducing CF cost[23].

A simple fiber spinning method, electrospinning, is extensively employed to yield micro- or nanofibers for lignin. Electrospinning utilizes electrostatic force to rapidly stretch the polymer solution ejected from a spinneret into a fine jet, which is subsequently deposited on a conductive collector [24]. Electric field can be introduced by applying a high voltage on the spinneret while grounding the collector. One of the challenges that need to be addressed for electrospun LBCF is its relatively poorer mechanical properties due to the amorphous structure[9], unique functional groups[25], and impurities of lignin[26], such as high sulfur content, ash content, or carbohydrates. Mechanical properties of electrospun LBCF reported in most recent works meet general purpose grade with low strength and modulus[27–29]. It is consequential to improve the mechanical properties of electrospun LBCF for a wide range of applications that require both ultrafine fibers and high mechanical performance. The potential applications include supercapacitors, fuel cells, adsorbent materials, etc.[30,31] Kumar et al.[30] and Wang et al.[31] indicated that the high specific surface area of the ultrafine fibers substantially improved the power density and the specific capacitance in supercapacitor application while good mechanical properties were favored for cycling stability. The high specific surface area also enhances the electrocatalytic response in fuel cell application with great durability ensured by high mechanical performance. In adsorption of volatile organic compounds, highly porous electrospun LBCF exhibits remarkable adsorption capacity and high strength provides good recyclability[31]. Several approaches have been reported to improve the mechanical properties of electrospun LBCF. Li et al. presented a fractionation method for lignin structure using laccase HBT enzyme, and replaced PAN up to 50 wt%, producing CF with 5% increase in elastic modulus than pure PAN CF[32]. The authors further demonstrated that lignin with high molecular weight was essential to improve mechanical properties of CF[33]. A steam-exploded

straw lignin with Poly(e-caprolactone) (PCL) binder could increase the elastic modulus as the lignin content increased, but this simultaneously caused reduction in the tensile strength[34]. Ding et al. reduced the viscosity of organosolv lignin/PAN mixture with butyric acid to produce CF. Tensile strength was increased by 104% which, however, was accompanied by fiber fusion induced by increment in the mobility of lignin during thermal stabilization[27]. While showing some success in improving mechanical properties, these aforementioned methods still increase the precursor cost of the end product, CF, due to the partial use of PAN.

An alternative strategy to improve the mechanical properties of LBCFs is aligning fibers, via good control and fundamental understanding of processing parameters, during the electrospinning process. Depending on the configuration of the collector, different types of fibers and fiber mats can be collected including random and aligned fibers. Aligned fibers can be achieved by various collectors, such as rotating apparatus, magnetic device, or electrodes[35–37]. Aligning fibers in electrospinning broadens the potential applications of ultrafine fibers as they could lead to improved mechanical properties compared to random fibers. Furthermore, in tissue regeneration, aligned fibers are generally adopted as cell scaffolds when directional growth of cells is favored[38]. In drug delivery, aligned fibers can maintain more constant and continuous release of drugs[39]. Aligned fibers are also preferred as piezoelectric material for better voltage generation[40], as energy device for stronger electrical response[41], and as fuel cell electrode for improved conductivity[42]. Aligning fibers is propitious for yielding high performance LBCF. Linearizing polymer chain is a promising solution that can overcome the limitation of the heterogeneous lignin structure, increasing crystallinity and mechanical performance of LBCFs[32]. Kakade et al. reported that aligning nanofibers macroscopically in electrospinning promoted alignment of molecular chains along the fiber orientation[43]. Aligning fibers was also shown to tailor physical features to form nanotube or nanowire structures[44], or to enhance uniaxial properties of fibers[45]. Ra et al. achieved substantial anisotropic electrical conductivity and directional dispersion of reinforcing fillers by aligning electrospun fibers[46]. Herrera et al. showed that aligning led to thinner electrospun fibers but multiple parameters, such as applied voltage and gap distance, were discovered to affect fiber alignment[47]. Aligned fibers typically exhibit enhanced mechanical properties since thinner fibers are less susceptible to defects while loads are distributed more uniformly along the uniaxially oriented fibers[48,49]. Wang and Chen validated the improvement of mechanical properties for aligned fibers by producing aligned hordein/zein fibers that exhibited tensile strength around 4 times higher than random fibers[50]. Similar results were obtained by Hossain et al., who demonstrated that electrospun PAN membranes showed higher strength, higher stiffness, and reduced extensibility after alignment[51]. By virtue of these advantages, Lin et al. fabricated LBCFs from fractionated lignin[52]. After aligning, the tensile strength of LBCFs was enhanced by 32% and elastic modulus by 175%. Even though the constructed LBCFs possessed excellent mechanical properties, their fractionation process required harsh acid treatment.

To ensure superior mechanical performance of LBCFs, optimization of the electrospinning process is required. Several studies have reported main factors affecting fiber diameter in electrospinning, namely flow rate, collection duration, tip-to-collector distance, applied voltage, spinning angle, charge density, and solution properties[53–55]. A few of these parameters also influence fiber

alignment and mechanical properties[47,56]. Despite these works, to date a systemic investigation on the optimization of electrospinning parameters for aligned lignin fiber generation is still absent. Aligning fibers to improve mechanical properties of electrospun LBCF is a cost-efficient method to yield high-quality submicron CFs with reduced precursor cost. The present work reports optimization for aligned lignin fiber generated by electrospinning, with the aim of both minimizing fiber diameter and maximizing mechanical performance. Box Behnken Design (BBD) was selected for the optimization since it provides adequate estimation for interacting effects with high efficiency[57]. This work not only presents a model to comprehensively explain the relationship between the parameters used in electrospinning and the properties of the produced aligned fibers, but also illustrates the effectiveness of alignment in increasing the performance of LBCF.

Experimental
Materials
Lignin powders with properties characterized in our previous work[58] were extracted from West Fraser Pulp Mill, processed by Innotech (Alberta), and dried at 100°C under vacuum to remove moisture[59]. Polyethylene oxide (PEO) (1000 kDa Mw) and anhydrous *N, N*-Dimethylformamide (DMF) were obtained from Sigma Aldrich (Canada).

Solution Preparation and Electrospinning
Adopting the method from our previous work, solution with total solid concentration of 22 wt% and lignin/PEO ratio of 95/5 was prepared[59]. The solution was loaded to a 10 mL syringe and discharged at flow rate of 420-460 nl/s by a syringe pump (Geneq Inc., Canada). The positive electric field applied on the 20G needle was maintained between 65 kV/m and 80 kV/m using a high voltage supply (ES100, GAMMA High Voltage Research, Ormond Beach, FL, USA) with a spinning gap of 20 cm. A customized rotating drum was used at 2000 to 3000 rpm. The rotating drum was wrapped around by an aluminum foil coated with release agent (Dupont® Teflon silicone lubricant) for fiber collection. The release agent facilitated the removal of fiber mats from the aluminum foil. The schematic of the setup for electrospinning and, subsequently collected aligned fibers is shown in Figure 1.
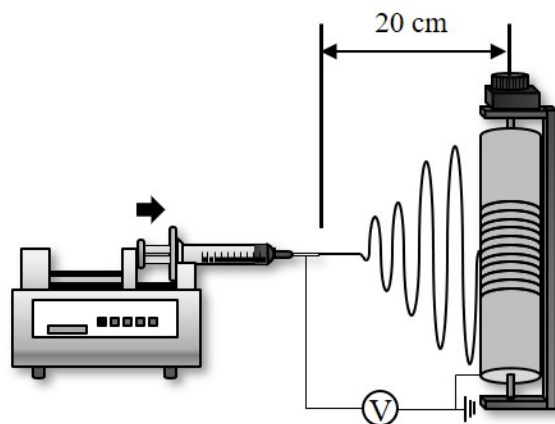

Figure 1. Schematic of electrospinning setup for aligned fibers.

Thermostabilization and Carbonization

The aligned electrospun fiber mats were thermostabilized using a tube furnace (OTF-1500X-III-UL) under atmospheric air. The chamber was heated at 0.5°C/min from room temperature to 250°C and held at this temperature for 1 hour. Oxidative thermostabilization removed the volatile content and hindered fiber fusion during the carbonization stage. The thermostabilized sample was subsequently carbonized at 1000°C (heating rate of 5°C/min) under Argon in the tube furnace. The target temperature was maintained constant for 1 hour. Mass yield of carbonization was calculated by comparing the weight of electrospun and carbonized specimen.

Scanning Electron Microscopy (SEM)

Morphology and fiber diameter of the specimens were characterized by SEM (Zeiss EVO MA 10, Oberkochen, Germany) with magnification of 500-1500x and accelerating voltage of 20 kV. The specimen was gold-coated with DESK II Gold Sputtering Unit (Denton Vacuum, Moorestown, USA). The SEM images were processed in ImageJ/Fiji analysis software (NIST, version 1.52 p). Fiber diameter and angle were reported as "mean ± standard deviation" by measuring at least 100 fibers from each SEM specimen. The fiber angle was first defined as the smallest angle between each fiber and a global reference line. The collected data were placed into bins between 0° and 90°. The orientation measured with the highest probability was then reset to 0° fiber angle and all the bins were shifted accordingly to obtain the fiber angle distribution. Fibers with angles within ±10° were considered as aligned fibers. Alignment percentage (%) was calculated as the ratio between the number of aligned fibers and the total number of measured fibers.

Optimization

Polymer concentration and electric field were optimized for electrospinning of random fibers in our previous work[59]. Electric field, flow rate, and rotating speed were analyzed for optimization in the present study, with the objectives of reaching small fiber diameter, high elastic modulus and tensile strength, and high alignment. Box-Behnken design (BBD) was employed for efficient analysis of main and interactive effects of parameters in quadratic model fitting[57]. BBD also assured accuracy of the model by removing the test runs with extreme values, for example, when all parameters were at their low level[57]. Repeated center points were used to assess the test reproducibility. The optimization was conducted in Design Expert® (Stat-Ease. v11).

Raman Spectroscopy

Degree of graphitization of the CF specimens was characterized using inVia Raman microscope (Renishaw plc, Wotton-under-Edge- Gloucestershire, UK) with 532 nm laser, exposure time of 4 s, 20 accumulations, laser power of 10%, grating of 1200 l/mm, and objective lens of 20x magnification. Raman spectra was recorded in Wire 5.3 software and analyzed using Origin 2020. Baseline correction was conducted for the data between wavenumbers of 800 and 1800 cm^{-1}. Then Gaussian curve fitting was used to find D band and G band, as well as their full width at half maximum (FWHM). I_D/I_G was obtained from the intensity ratio and the area ratio between the D band and the G band.

Mechanical Characterization

Each rectangular tensile specimen of lignin fiber mat with the testing direction aligned with the most probable fiber direction was placed within a "[" shaped paper holder to mitigate stress

concentration at the edge of test clamps. For each combination of electric field, flow rate, and rotating speed, tensile test was conducted on at least 10 specimens by an ElectroForce 3200 Series III tensile machine (Bose Corporation) equipped with a 250 g load cell. Specimens were tested at 0.01 mm/s strain rate and had 30 mm gauge length. The testing environment was held around 25°C and 25% relative humidity. The specific stress was calculated from the applied force by [60]

$$\text{Specific stress (g/tex)} = \frac{\text{Load (g)}}{\text{width (mm)} \times \text{areal density (g/m}^2)} \quad [1]$$

Areal density (g/m^2) was obtained by dividing mass (g) by width (m) and length (m). Then the specific stress was converted into stress in MPa by multiplying it with the gravitational acceleration (9.81 m/s^2) and the bulk density, which is 1.35 g/cm^3 for lignin or 1.70 g/cm^3 for carbon. In this approach, the stress is given by,

$$\text{Stress} = \frac{\text{Load}}{\frac{\text{Mass of fiber mat}}{(\text{bulk density of fiber}) \times (\text{length of fiber mat})}} = \frac{\text{Load}}{\text{Cross sectional area of fibers}} \quad [2]$$

The cross-sectional area of the fibers is considered instead of the cross-sectional area of the mat to exclude the effects of porosity and density of the fibers mat.

Results and Discussion

Morphology and alignment analysis of lignin fibers

SEM images of the aligned electrospun lignin fibers and carbonized fibers are presented in Figure 2a-d in comparison to the random lignin fibers (Figure 2e). The fibers are smooth, compactly distributed, and predominately aligned, while fiber fusion (Supporting Information-Figure S1a) and layer separation (Supporting Information-Figure S1b) are observed in some areas. At low rotating speed of 2000 rpm (Figure 2a), the fiber angle distribution is wider with a flatter peak and larger standard deviation (±31.38°). At high rotating speed of 3000 rpm (Figure 2b), the fiber angle distribution is narrower with a sharper peak and smaller standard deviation (±25.86°). The results suggest that fibers are more oriented at higher rotating speed. The presence of unaligned fibers may be induced by the air circulation exerted on the ejected jet by the rapid drum rotation. Figure 2c shows the morphology of the bottom surface contacting the aluminum foil coated with release agent for the fibers electrospun at 2000 rpm. Compared to the top surface (Figure 2a), fiber angle distribution shows smaller standard deviation (±27.89°), indicating fibers closer to the collector are more aligned.
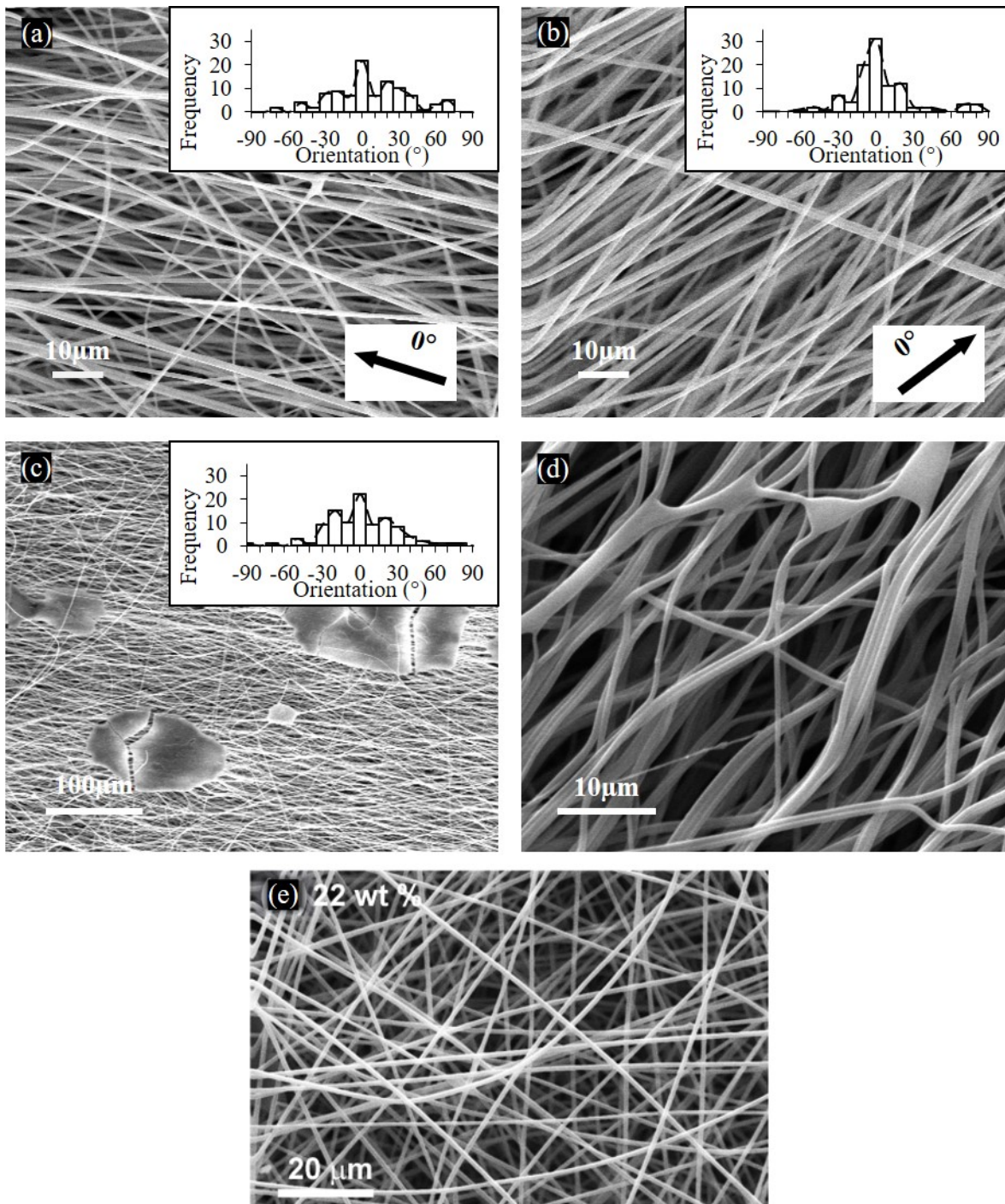
Figure 2. Fiber morphology of as-spun aligned lignin fibers at electric field of 65 kV/m, flow rate of 440 nl/s, rotating speed of (a) 2000 rpm and (b) 3000 rpm, with sample defects of (c) release agent residue, (d) fusion and curvy fibers after carbonization, and (e) random lignin fibers reproduced from previous work[59].

Parameter Optimization

The electrospinning parameters were optimized via BBD with two extra center points as shown in Table 1. A total of 15 test runs were conducted to perform the optimization, with electric field (F), flow rate (FR) and rotating speed (S) being the investigated parameters. The coded values (-1, 0, +1) correspond to low, center, and high levels of electric field (65, 72.5, 80 kV/m), flow rate (420, 440, 460 nl/s), and rotating speed (2000, 2500, 3000 rpm). Electric field and flow rate lower than the analyzed ranges were incapable of producing continuous spinning, while higher levels induced electrospraying at the collector. Fibers electrospun at rotating speed lower than 2000 rpm were mostly random, whereas 3000 rpm is the maximum rotating speed for the customized rotating drum due to vibration concern. Alignment percentage (A), average fiber diameter (D), elastic modulus (E), and tensile strength (σ) were chosen as the response variables. The goal of the optimization was set to maximize alignment, minimize fiber diameter, maximize elastic modulus, and maximize tensile strength.

Table 1. Design matrix of dependent variables in coded values (subscripted c) and the corresponding responses in actual values (subscripted a) for aligned lignin fiber mats

Test Run	Coded Variables			Responses			
	F_c	FR_c (nm)	S_c (nm)	A_a (%)	D_a (nm)	E_a (MPa)	σ_a (MPa)
1	+1	+1	0	58%	946.48	807.50	7.98
2	+1	0	+1	62%	900.46	799.64	6.90
3	+1	0	-1	37%	907.01	940.67	11.20
4	+1	-1	0	43%	900.40	886.83	10.54
5	0	0	0	58%	895.79	979.13	8.75
6	0	0	0	43%	1010.97	928.43	8.16
7	0	0	0	44%	978.60	899.34	8.33
8	0	-1	-1	55%	1045.12	890.06	9.19
9	0	+1	+1	45%	1026.63	605.61	8.67
10	0	+1	-1	48%	983.17	791.32	7.71
11	0	-1	+1	52%	980.07	786.47	9.51
12	-1	+1	0	40%	1135.3	717.11	7.77
13	-1	0	-1	36%	1023.51	806.49	7.42
14	-1	0	+1	62%	1149.09	782.08	5.07
15	-1	-1	0	35%	1183.52	817.27	8.09

The model summary generated from Design Expert® based on the design matrix is listed in Table 2. Quadratic regression model given by Equation [2] was used to fit the data, where $\hat{y}$ is the

response, x_i is the ith factor, β_i is the regression coefficient associated with the effect of x_i, and β_{ij} is the regression coefficient associated with the interaction effect between x_i and x_j.

$$\hat{y} = \beta_0 + \beta_1 x_1 + \beta_2 x_2 + \beta_3 x_3 + \beta_{12} x_1 x_2 + \beta_{13} x_1 x_3 + \beta_{23} x_2 x_3 + \beta_{11} x_1{}^2$$
$$+ \beta_{22} x_2{}^2 + \beta_{33} x_3{}^2 \qquad [2]$$

The quadratic model reduced to the linear model when the regression coefficients β_{ij} were set to zero. For 2FI (two-factor-interaction) model, the coefficients of high order terms, $\beta_{11}, \beta_{22},$ and β_{33}, were set to 0. Cubic terms were also added to Equation [2] but the model showed aliased structure. When the response is alignment percentage, all models are insignificant as p-value is large for the suggested model. Therefore, alignment percentage is not considered in further optimization. When the response is fiber diameter or tensile strength, linear model shows low p-value (p<0.05), high adjusted R^2, and high predicted R^2, indicating that the model is statistically significant. When the response is elastic modulus, quadratic model shows the best performance. The selected predictive models for each response with both coded and actual values are shown in Supporting Information-Table S1. The models evaluate how the electrospinning parameters and alignment quantitatively affect the properties of the electrospun lignin fibers. It is a key contribution to future works on improving the mechanical properties of LBCFs.

Table 2. Models recommended for each response of aligned lignin fiber mats

Response	Source	Sequential p-value	Adjusted R^2	Predicted R^2	Remarks
A	Linear	0.2810	0.0882	-0.4200	Recommended
	2Fi	0.9698	-0.2178	-2.2257	
	Quadratic	0.9009	-0.7519	-7.4380	
	Cubic	0.2613	0.1993		Aliased
D	Linear	0.0054	0.5796	0.3964	Recommended
	2FI	0.0973	0.7263	0.6036	
	Quadratic	0.5303	0.7081	0.2734	
	Cubic	0.7989	0.5207		Aliased
E	Linear	0.0437	0.3734	0.2376	
	2FI	0.8646	0.2101	-0.1759	
	Quadratic	0.0083	0.8577	0.5408	Recommended
	Cubic	0.6533	0.8199		Aliased
σ	Linear	0.0391	0.3869	-0.0252	Recommended
	2FI	0.6844	0.2931	-1.1241	
	Quadratic	0.6800	0.1426	-3.8153	
	Cubic	0.0299	0.9571		Aliased

The above models were evaluated using analysis with variance (ANOVA) for fiber diameter (Table 3), elastic modulus (Table 4), and tensile strength (Supporting Information-Table S2). All parameters without subscripts below are in coded values. Adequate precision, in terms of the signal-to-noise ratio, should be larger than 4 for the model to be significant. P-value lower than 0.05 demonstrates a term in the model is significant. For both fiber diameter and tensile strength, F is the only significant factor. For elastic modulus, the significant factors or factor interactions are FR^2, FR, S, S^2 and F.

Table 3. ANOVA analysis of model (coded) for fiber diameter

Source	Sum of Squares	df	Mean Square	F-value	p-value
Model	88809.03	3	29603.01	10.22	0.0016
F	87583.68	1	87583.68	30.23	0.0002
FR	38.41	1	38.41	0.0133	0.9104
S	1186.94	1	1186.94	0.4097	0.5352
Residual	31866.58	11	2896.96		
Lack of Fit	24809.40	9	2756.60	0.7812	0.6758
Pure Error	7057.18	2	3528.59		
Cor Total	120676	14			
User Std. Dev.	210.47			R^2	0.7359
Std. Dev.	53.82			Adjusted R^2	0.6639
Mean	1004.41			Predicted R^2	0.5375
C.V. %	5.36			Adequate Precision	8.4055

Table 4. ANOVA analysis of model (coded) for elastic modulus

Source	Sum of Squares	df	Mean Square	F-value	p-value
Model	120300	9	13366.18	10.38	0.0095
F	12144.53	1	12144.53	9.43	0.0278
FR	26346.14	1	26346.14	20.46	0.0063
S	25848.22	1	25848.22	20.07	0.0065
F*FR	108.51	1	108.51	0.0842	0.7833
F*S	3400.11	1	3400.11	2.64	0.1651
FR*S	1686.09	1	1686.09	1.31	0.3044
F^2	3852.08	1	3852.08	2.99	0.1443
FR^2	34137.18	1	34137.18	26.50	0.0036

S²	18671.28	1	18671.28	14.50	0.0125
Residual	6440.00	5	1288.00		
Lack of Fit	3178.54	3	1059.51	0.6497	0.6533
Pure Error	3261.46	2	1630.73		
Cor Total	126700	14			

User Std. Dev.	263.45	R²	0.9492
Std. Dev.	35.89	Adjusted R²	0.8577
Mean	829.20	Predicted R²	0.5408
C.V. %	4.33	Adequate Precision	11.0423

The fitted models were validated in Figure 3a-c by plotting the predicted vs. actual responses, and in Figure 3d-f by plotting the residuals vs. predicted responses. Predicted values are close to actual values for all three responses, suggesting good model fitting. Dispersion of data is wider for fiber diameter and tensile strength, but no obvious outliers are present. The red horizontal lines are the upper and the lower limits of residuals. The residuals are independent of the predicted responses and no trend in data is observed, confirming the good quality of the model fitting.
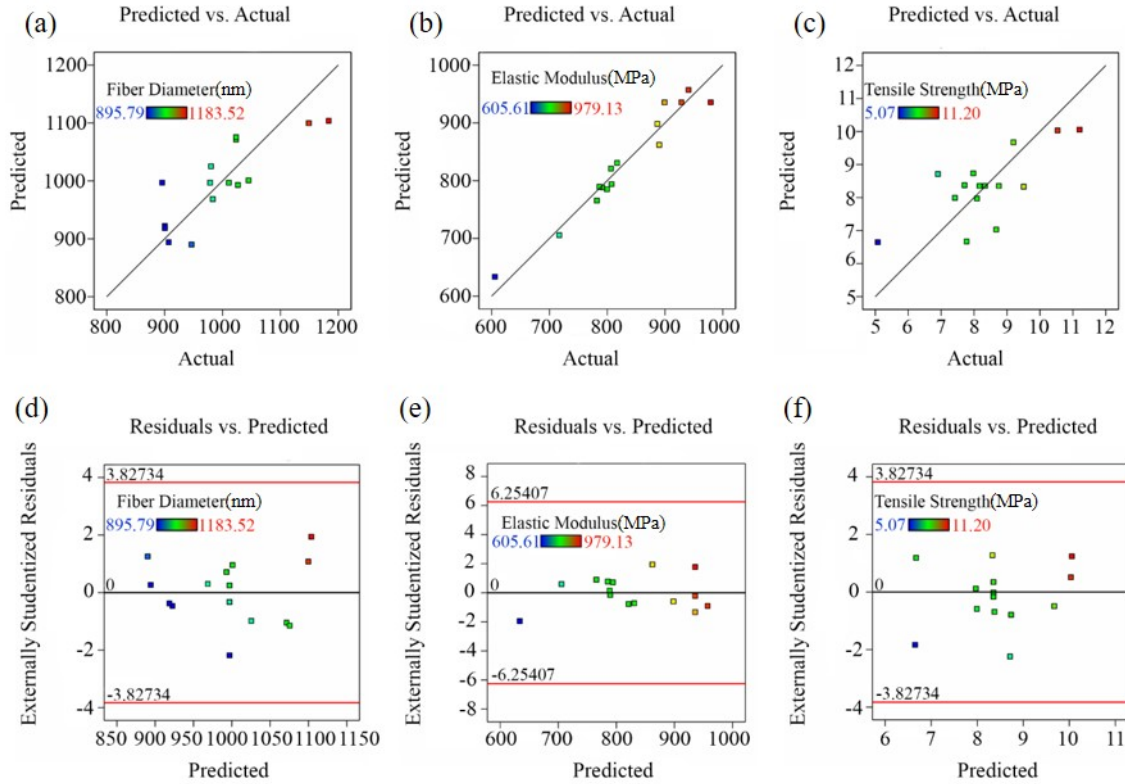
Figure 3. Predicted value vs. actual value for (a) fiber diameter and (b) elastic modulus (c) tensile strength. Residual vs. predicted value for (d) fiber diameter and (e) elastic modulus (f) tensile strength.

The main factor effect graphs, or perturbation plots, for fiber diameter (Figure 4a-c), elastic modulus (Figure 4d-f), and tensile strength (Figure 4g-i) are used to show the effect of each factor on the response while keeping other factors constant. Fiber diameter decreases with F, which is because fibers are stretched more under higher electric field. For FR and S, fiber diameter shows slightly negative and positive correlations, respectively, but their variations are negligible (p-value > 0.05). Tensile strength increases with F, which can be attributed to finer fibers achieved at higher electric field. The correlation between tensile strength and the other two parameters are insignificant as demonstrated in previous ANOVA analysis. Elastic modulus exhibits polynomial relationship with three parameters. The highest elastic modulus is obtained at center levels of F (72.5 kV/m), FR (440 nl/s), and S (2500 rpm).

Two-factor interaction effects on the elastic modulus (Figure 5) are analyzed by keeping the third parameter constant. The plots for fiber diameter and tensile strength are straight lines due to the recommended linear regression model and are not illustrated here. At constant S, elastic modulus reaches highest point with high range of F (72.5-80 kV/m) and low range of FR (420-440 nl/s). Therefore, elastic modulus shows an overall positive trend with F and negative trend with FR. At constant F, the peak of elastic modulus lies around medium to low range of S (2000-2500 rpm) and FR, indicating elastic modulus generally decreases with S. Since the investigated range of flow rate is high, the enhancement of mechanical properties with more oriented fibers may have

12

saturated around 2000 rpm. Further increase in rotating speed may generate large air flow and vibration, causing decrease in fiber deposition. Ayres et al. also demonstrated that tensile properties of electrospun fibers did not increase indefinitely with rotating speed[61], which agrees with our finding. At constant FR, maximum elastic modulus is found at high level of F and low level of S.
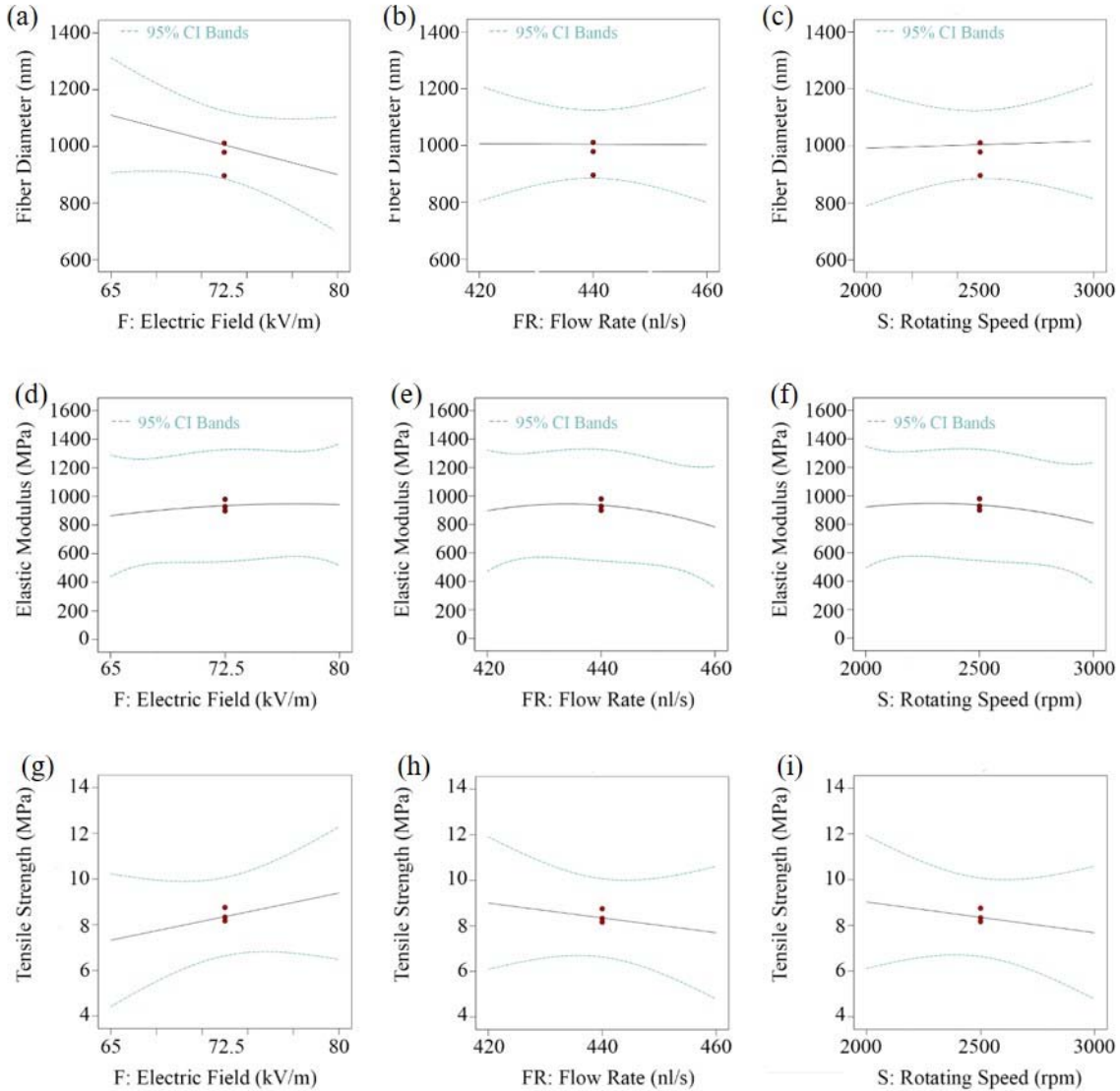

Figure 4. Main effects of (a, d, g) electric field, (b, e, h) flow rate, and (c, f, i) rotating speed on (top) fiber diameter, (middle) elastic modulus and (bottom) tensile strength.
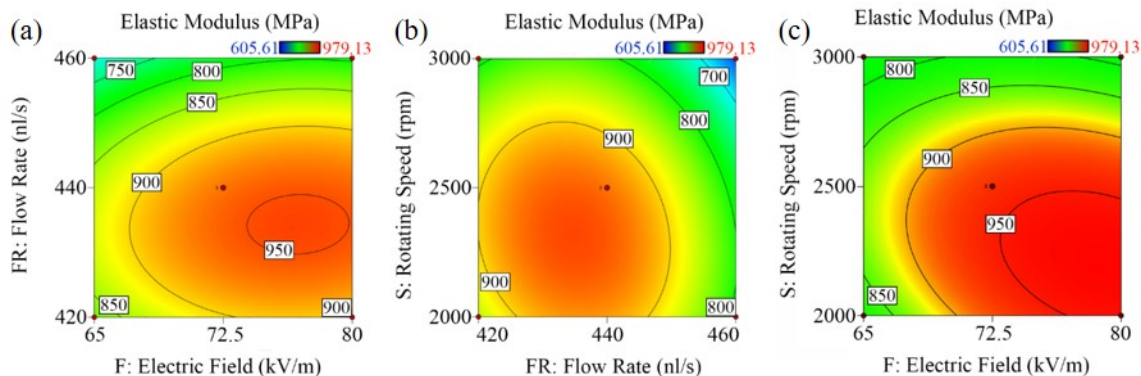
Figure 5. Interaction effects on the elastic modulus between (a) electric field and flow rate, (b) flow rate and rotating speed, (c) electric field and rotating speed.

The goal and the range of each variable in the optimization are shown in Supporting Information-Table S3. Ranges of the variables were selected based on lower and higher limits of the corresponding experimental data. Importance was used to assign desirability of each goal such that the optimized condition may be adjusted to favor one goal than another. It was set to default (3) for all goals in this study. After optimization, three conditions were recommended (Table 5). The condition with the highest desirability (electric field of 80 kV/m, flow rate of 440 nl/s, rotating speed of 2000 rpm) was considered as the optimal electrospinning condition. In compared to experimental data (tensile strength of 11.20±3.02 MPa, elastic modulus of 940.67±182.41 MPa, fiber diameter of 907.01±147.44 nm), the predicted responses (tensile strength of 10 MPa, elastic modulus of 957 MPa, fiber diameter of 888 nm) show excellent agreement.

Table 5. Optimal parameters for electrospinning aligned lignin fibers

Number	Optimum parameters			Predicted response			Desirability	
	Electric Field	Flow Rate	Rotating Speed	Tensile Strength	Elastic Modulus	Fiber Diameter		
1	80	440	2000	10	957	888	0.669	Selected
2	80	420	2000	11	893	890	0.661	
3	80	440	2500	10	942	900	0.638	

Aligned lignin fibers were electrospun at the optimal electrospinning condition from Table 8 and subsequently carbonized. Carbonization mass yield was 47%. Some fiber orientations were lost due to relaxation[62] and curvy fibers were produced after carbonization of aligned fibers along with substantial fiber fusion (Figure 2d). To determine the effect of fiber alignment on mechanical properties of the electrospun fibers, random fibers were collected with release agent at electrospinning condition optimized in previous work[59]. Comparing average fiber diameter (Table 6), fiber diameter reduced to 60% of its original size from random to aligned lignin electrospun fibers, then decreased to 77% of aligned fiber diameter after carbonization.

Table 6. Average fiber diameter and fiber morphology of random lignin fibers, aligned lignin fibers, and aligned carbon fibers, all produced with the presence of release agent (Teflon).

Lignin	Morphology	Diameter (nm)
Random lignin fibers	Bead-free, fusion	1509.68 ± 177.57
Aligned lignin fibers	Mostly bead-free, fusion	907.01 ± 147.44
Aligned carbon fibers	Mostly bead-free, fusion	697.07 ± 96.41

Raman Spectroscopy

The degree of graphitization for both random and aligned LBCFs produced with their respective optimized parameters was characterized. From the Raman spectra in Figure 6a, two peaks were observed corresponding to D band and G band. G band is associated with Raman scattering of sp^2 carbon bonds, typically an indication of ordered graphite crystallite structures[63,64]. D band is commonly recognized as denotation of defects or disordered structure[64]. After aligning LBCFs, average D band position shifted from 1339 cm^{-1} to 1344 cm^{-1} while G band position stayed almost constant at ~1582 cm^{-1} (Figure 6b). Higher frequency and sharper peak of D band were also reported by Torres-Canas et al.[65] as the carbonization temperature was increased for LBCFs. The finding was attributed to increased formation of 6-order carbon aromatic rings[66]. Compared with random LBCFs, aligned LBCFs showed a similar D band FWHM but an increase in G band FWHM (Figure 6c), suggesting broadening distribution of nonaromatic conjugated structure[67]. Insignificant change in I_D/I_G (area) and I_D/I_G (intensity) in Figure 6d indicated alignment did not change the composition of amorphous carbon structures.
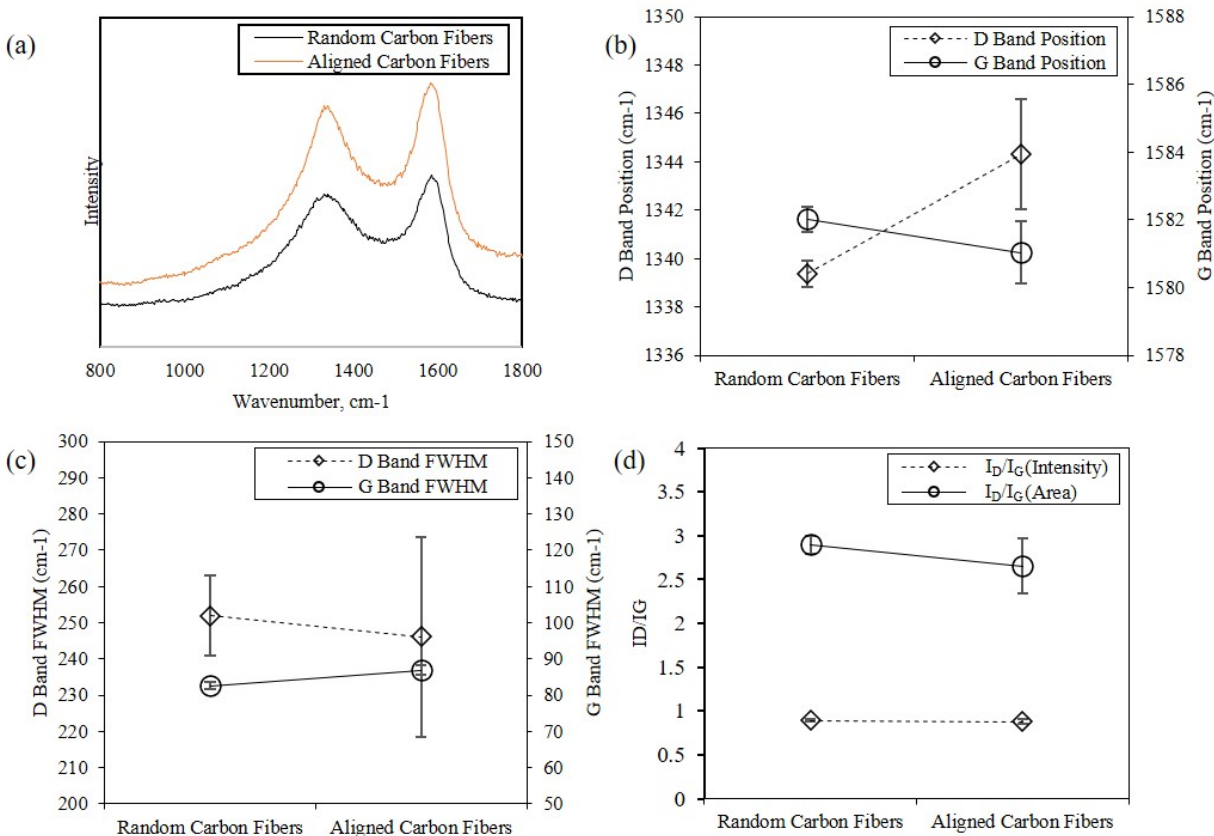
Figure 6. (a) Raman spectra of random[*] and aligned CFs, (b) D and G band positions, (c) D and G band FWHM, (d) I_D/I_G of random and aligned LBCFs

Mechanical Characterization

Mechanical properties of electrospun and carbonized aligned lignin fibers produced with the optimized parameters were characterized and compared to previously reported mechanical properties of random lignin fibers[59]. Stress strain curves for aligned LBCFs (Supporting Information-Figure S2) show tensile strength of 18.78±6.11 MPa (1.7 times of aligned as-spun lignin fibers) and elastic modulus of 3145.47±917.75 MPa (3.3 times of aligned as-spun lignin fibers). From Figure 7, there is some resemblance in data trends for tensile strength and elastic modulus. After aligning at 2000 rpm, tensile strength and elastic modulus show 16.7 times and 10.7 times improvement than random LBCFs. During a uniaxial loading, random fibers first re-orient towards the loading direction. Some fibers along the loading axis break first and transfer the load to the re-oriented fibers. This uneven load transfer reduces the effective cross-sectional loading area, resulting in weaker mechanical properties. On the other hand, the aligned fibers can carry the load more uniformly and alleviate the effect of fiber re-orientation. It should be noted that the aligned lignin fibers produced under the optimal condition had 37% of alignment, which was not a very high value. However, this moderate increase in alignment led to substantial

---

[*] Data reported in our previous publication (add ref)

16

improvement in mechanical properties. The manufactured LBCF is suitable for general purpose grade CF.

Spray residues, visible from Figure 2c, form cracking islands fusing neighboring fibers. Approximately 60% of the fibers on the bottom surface were free of spray residues. These islands of spray residues negatively affected the force distribution on the fibers in tensile loading. In addition, the diameter of random lignin fibers collected with the presence of release agent was up to 1.5 times that of random fibers collected without release agent. This is because the sprayed released agent formed an insulating layer on the substrate, affecting the electric field. The increase in fiber diameter caused tensile strength and elastic modulus to decrease to 32% (Figure 7a) and 38% (Figure 7b) respectively of their original values for random fibers collected without release agent[59]. In conclusion, it is expected that the mechanical properties of aligned LBCFs can be further enhanced if the use of release agent could be avoided. However, it remains a challenge to produce aligned LBCFs without release agent using our in-house built electrospinning set up. Future investigation into replacement of release agent to facilitate collection of lignin fibers without compromising the mechanical properties is required.

The highest alignment percentage achieved in this study was 62% as shown in Table 1, with rotating speed of 3000 rpm. Even though increasing the rotating speed posed a positive effect on fiber alignment, improvement of fiber alignment with the rotating speed reached its limit at around 2000 rpm due to vibrations observed in the in-house built cost-effective rotating drum used in this work. Commercial rotating drums are better in terms of reducing vibration and rotational disturbance that can affect the trajectory of the ejected jet. However, cost of these commercial rotating drums is a concern in terms of producing inexpensive LBCF. Further enhancement in alignment can be achieved by reducing the vibration of equipment in future investigations.

Aligned fibers with superior mechanical properties can be applied as interlaminar reinforcement for composites[68]. For instance, addition of semi-aligned carbon nanofiber in epoxy resin matrix can increase the bending modulus by 200% and the bending strength by 175%[69]. Aligned carbon nanofibers can also be used as electrolyte for fuel cell application to improve proton conductivity via alignment[70] and great mechanical performance ensures the system integrity and robustness[71]. The thorough analysis in this work on the effect of electrospinning parameters demonstrated how the properties of LBCFs may be tailored. Future researchers can adopt these optimized parameters to produce LBCFs with desirable performance for various applications.
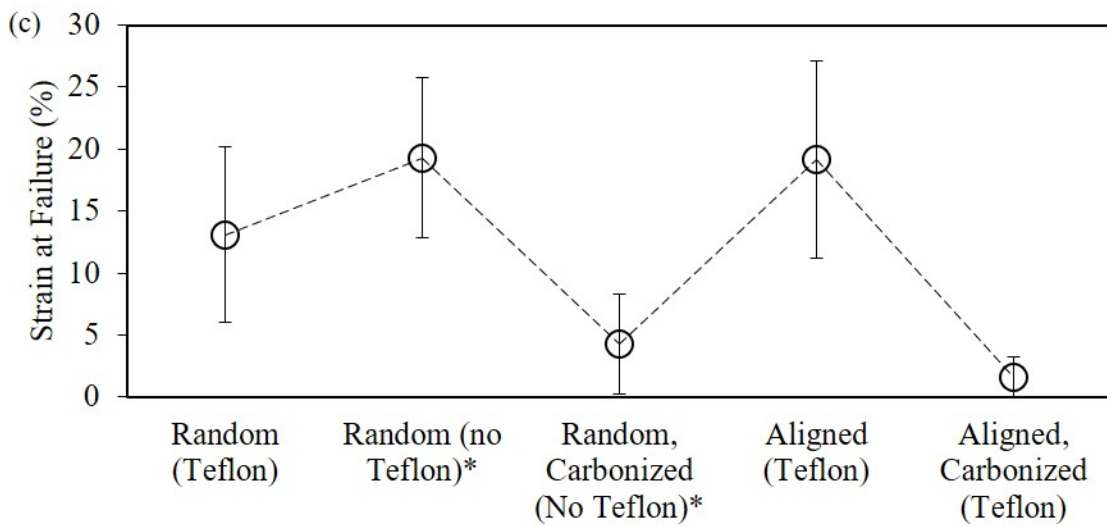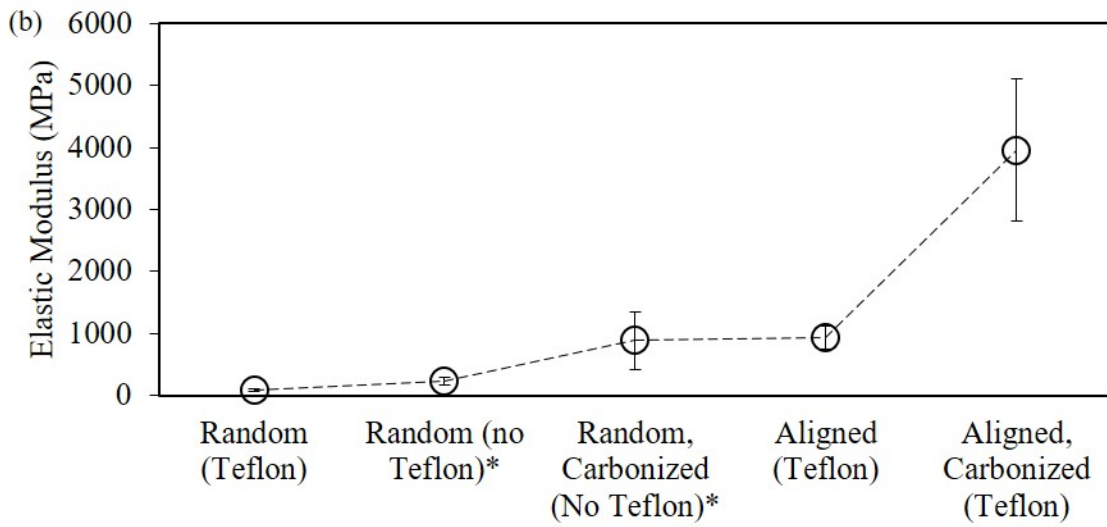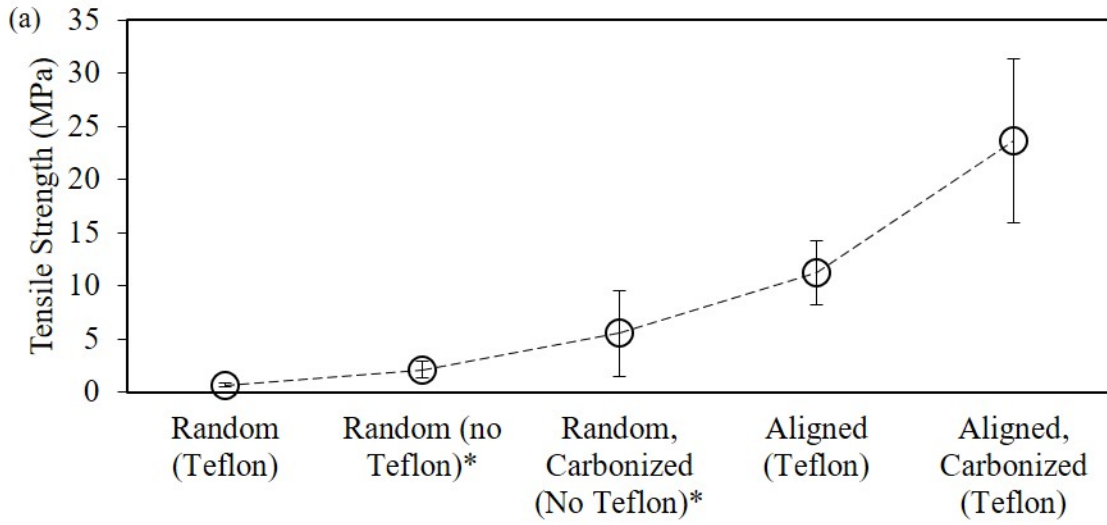
Figure 7. Comparison of (a) tensile strength, (b) elastic modulus, and (c) strain at failure for as-spun and carbonized lignin fiber mats with and without alignment or release agent (*data reported in previous work [59])

Conclusion

Aligned lignin-based carbon fibers were obtained and optimized using electrospinning technique. The electrospinning parameters played a significant role in controlling fiber morphology and mechanical properties of the end-product. Using the Box-Behnken method, the smallest fiber diameter (894 nm) and highest mechanical properties (tensile strength of 10 MPa and elastic modulus of 957 MPa) for aligned electrospun lignin material were achieved at the following optimal parameters: electric field of 80 kV/m, flow rate of 440 nl/s, and rotating speed of 2000 rpm. At this optimal experimental condition, average fiber diameter of aligned lignin carbon fibers decreased 77% compared to random lignin carbon fibers, with 16.7 times improvement in tensile strength, and 10.7 times improvement in elastic modulus. The substantial improvement in mechanical properties highlighted the effectiveness of alignment in manufacturing environmentally-friendly and cost-effective carbon fibers with good mechanical performance.

Nomenclature List

BBD   Box-Behnken Design
CF   Carbon Fiber
D   Average Fiber Diameter
DMF   *N, N*-Dimethylformamide
E   Elastic Modulus
F   Electric Field
FR   Flow Rate
LBCF Lignin-based Carbon Fiber
Mw   Molecular Weight
PEO   Polyethylene oxide
S   Rotating Speed
σ Tensile Strength

References

1. Aoki, K.; Usui, Y.; Narita, N.; Ogiwara, N.; Lashigaki, N.; Nakamura, K.; Kato, H.; Sano, K.; Ogiwara, N.; Kametani, K.; Kim, C.; Taruta, S.; Kim, Y. A.; Endo, M.; Saito, N. *Small* **2009**, *5*, 1540.
2. De Rosa, I. M.; Sarasini, F.; Sarto, M. S.; Tamburrano, A. *IEEE Trans. Electromagn. Compat.* **2008**, *50*, 556.
3. Jost, K.; Stenger, D.; Perez, C. R.; McDonough, J. K.; Lian, K.; Gogotsi, Y.; Dion, G. *Energy Environ. Sci.* **2013**, *6*, 2698.
4. Hu, S.; Zhang, S.; Pan, N.; Hsieh, Y. Lo *J. Power Sources* **2014**, *270*, 106.
5. Wang, S. X.; Yang, L.; Stubbs, L. P.; Li, X.; He, C. *ACS Appl. Mater. Interfaces* **2013**, *5*, 12275.
6. Ding, R.; Wu, H.; Thunga, M.; Bowler, N.; Kessler, M. R. *Carbon N. Y.* **2016**, *100*, 126.
7. Kim, C.; Yang, K. S.; Kojima, M.; Yoshida, K.; Kim, Y. J.; Kim, Y. A.; Endo, M. *Adv. Funct. Mater.* **2006**, *16*, 2393.
8. Beck, R. J.; Zhao, Y.; Fong, H.; Menkhaus, T. J. *J. Water Process Eng.* **2017**, *16*, 240.
9. Bengtsson, A.; Bengtsson, J.; Olsson, C.; Sedin, M.; Jedvert, K.; Theliander, H.; Sjöholm, E. *Holzforschung* **2018**, *72*, 1007.
10. Suzuki, M. *Carbon N. Y.* **1994**, *32*, 577.
11. Morgan, P. *Carbon fibers and their composites*; CRC press, **2005**.
12. Inagaki, M. *New carbons-control of structure and functions*; Elsevier, **2000**.
13. Mordkovich, V. Z. *Teor. Osn. Khimicheskoi Tekhnologii* **2003**, *37*, 460.
14. Park, S. J.; Seo, M. K. *Interface science and composites*; Academic Press, **2011**; Vol. 18.
15. Kaur, J.; Millington, K.; Smith, S. *J. Appl. Polym. Sci.* **2016**, *133*, 1.
16. Baker, D. A.; Gallego, N. C.; Baker, F. S. *J. Appl. Polym. Sci.* **2012**, *124*, 227.
17. Baker, D. A.; Rials, T. G. *J. Appl. Polym. Sci.* **2013**, *130*, 713.
18. Traceski, F. T. *Acquis. Rev. Q. - Spring Ind. Capab. Assessments Dir.* **1999**, 179.
19. Gellerstedt, G.; Sjöholm, E.; Brodin, I. *Open Agric. J.* **2010**, *4*, 119.
20. Hassan, M. M.; Schiermeister, L.; Staiger, M. P. *ACS Sustain. Chem. Eng.* **2015**, *3*, 2660.
21. Otani, S.; Fukuoka, Y.; Igarashi, B.; Sasaki, K. Method for Producing Carbonized Lignin Fiber **1969**.
22. Norberg, I.; Nordström, Y.; Drougge, R.; Gellerstedt, G.; Sjöholm, E. *J. Appl. Polym. Sci.* **2013**, *128*, 3824.
23. Kouisni, L.; Gagné, A.; Maki, K.; Holt-Hindle, P.; Paleologou, M. *ACS Sustain. Chem. Eng.* **2016**, *4*, 5152.
24. Worarutariyachai, T.; Chuangchote, S. **2020**, *15*, 2412.
25. Sahoo, S.; Misra, M.; Mohanty, A. K. *Compos. Part A Appl. Sci. Manuf.* **2011**, *42*, 1710.
26. Schlee, P.; Hosseinaei, O.; Baker, D.; Landmér, A.; Tomani, P.; Mostazo-López, M. J.; Cazorla-Amorós, D.; Herou, S.; Titirici, M. M. *Carbon N. Y.* **2019**, *145*, 470.
27. Ding, R.; Wu, H.; Thunga, M.; Bowler, N.; Kessler, M. R. *Carbon N. Y.* **2016**, *100*, 126.
28. Cho, M.; Karaaslan, M. A.; Renneckar, S.; Ko, F. *J. Mater. Sci.* **2017**, *52*, 9602.
29. Cho, M. J.; Ji, L.; Liu, L. Y.; M. Johnson, A.; Potter, S.; Mansfield, S. D.; Renneckar, S. *Ind. Crops Prod.* **2020**, *155*, 112833.
30. Kumar, M.; Hietala, M.; Oksman, K. *Front. Mater.* **2019**, *6*, 62.
31. Wang, S.; Bai, J.; Innocent, M. T.; Wang, Q.; Xiang, H.; Tang, J.; Zhu, M. *Green Energy Environ.* **2021**.
32. Li, Q.; Xie, S.; Serem, W. K.; Naik, M. T.; Liu, L.; Yuan, J. S. *Green Chem.* **2017**, *19*,

1628.

33. Li, Q.; Serem, W. K.; Dai, W.; Yue, Y.; Naik, M. T.; Xie, S.; Karki, P.; Liu, L.; Sue, H. J.; Liang, H.; Zhou, F.; Yuan, J. S. *J. Mater. Chem. A* **2017**, *5*, 12740.

34. Pucciariello, R.; Bonini, C.; D'Auria, M.; Villani, V.; Giammarino, G.; Gorrasi, G. *J. Appl. Polym. Sci.* **2008**, *109*, 309.

35. Teo, W. E.; Inai, R.; Ramakrishna, S. *Sci. Technol. Adv. Mater.* **2011**, *12*.

36. Sahay, R.; Thavasi, V.; Ramakrishna, S. *J. Nanomater.* **2011**, *2011*.

37. Yang, D.; Lu, B.; Zhao, Y.; Jiang, X. *Adv. Mater.* **2007**, *19*, 3702.

38. Liu, R.; Becer, C. R.; Screen, H. R. C. *Macromol. Biosci.* **2018**, *18*, 1.

39. Eslamian, M.; Khorrami, M.; Yi, N.; Majd, S.; Abidian, M. R. *J. Mater. Chem. B* **2019**, *7*, 224.

40. Edmondson, D.; Cooper, A.; Jana, S.; Wood, D.; Zhang, M. *J. Mater. Chem.* **2012**, *22*, 18646.

41. Azmi, S.; Hosseini Varkiani, S. M.; Latifi, M.; Bagherzadeh, R. *J. Ind. Text.* **2020**.

42. Simotwo, S. K.; Kalra, V. *Electrochim. Acta* **2016**, *198*, 156.

43. Kakade, M. V.; Givens, S.; Gardner, K.; Lee, K. H.; Chase, D. B.; Rabolt, J. F. *J. Am. Chem. Soc.* **2007**, *129*, 2777.

44. Frenot, A.; Chronakis, I. S. *Curr. Opin. Colloid Interface Sci.* **2003**, *8*, 64.

45. Borges, A. L. S.; Münchow, E. A.; de Oliveira Souza, A. C.; Yoshida, T.; Vallittu, P. K.; Bottino, M. C. *J. Mech. Behav. Biomed. Mater.* **2015**, *48*, 134.

46. Ra, E. J.; An, K. H.; Kim, K. K.; Jeong, S. Y.; Lee, Y. H. *Chem. Phys. Lett.* **2005**, *413*, 188.

47. Herrera, N. V.; Mathew, A. P.; Wang, L. Y.; Oksman, K. *Plast. Rubber Compos.* **2011**, *40*, 57.

48. Le, Q. P.; Uspenskaya, M. V.; Olekhnovich, R. O.; Baranov, M. A. *Fibers* **2021**, *9*, 1.

49. Lee, J.; Deng, Y. *Macromol. Res.* **2012**, *20*, 76.

50. Wang, Y.; Chen, L. *ACS Appl. Mater. Interfaces* **2014**, *6*, 1709.

51. Hossain, N.; De Silva, R.; Goh, K.-L.; Pasbakhsh, P. In *Electrospun Polymers and Composites*; Elsevier, **2021**; pp 361.

52. Lin, L.; Li, Y.; Ko, F. K. *J. Fiber Bioeng. Informatics* **2013**, *6*, 335.

53. Deitzel, J. M.; Kleinmeyer, J.; Harris, D.; Beck Tan, N. C. *Polymer (Guildf).* **2001**, *42*, 261.

54. Ali, A. A.; El-Hamid, M. A. *Compos. Part A Appl. Sci. Manuf.* **2006**, *37*, 1681.

55. Yun, K. M.; Suryamas, A. B.; Iskandar, F.; Bao, L.; Niinuma, H.; Okuyama, K. *Sep. Purif. Technol.* **2010**, *75*, 340.

56. Zhang, X.; Nakagawa, R.; Chan, K. H. K.; Kotaki, M. *Macromolecules* **2012**, *45*, 5494.

57. Ferreira, S. L. C.; Bruns, R. E.; Ferreira, H. S.; Matos, G. D.; David, J. M.; Brandão, G. C.; da Silva, E. G. P.; Portugal, L. A.; dos Reis, P. S.; Souza, A. S.; dos Santos, W. N. L. *Anal. Chim. Acta* **2007**, *597*, 179.

58. Ghosh, T.; Ngo, T. D.; Kumar, A.; Ayranci, C.; Tang, T. *Green Chem.* **2019**, *21*, 1648.

59. Ghosh, T.; Chen, J.; Kumar, A.; Tang, T.; Ayranci, C. *RSC Adv.* **2020**, *10*, 22983.

60. Hotaling, N. A.; Bharti, K.; Kriel, H.; Simon, C. G. *Biomaterials* **2015**, *61*, 327.

61. Ayres, C.; Bowlin, G. L.; Henderson, S. C.; Taylor, L.; Shultz, J.; Alexander, J.; Telemeco, T. A.; Simpson, D. G. *Biomaterials* **2006**, *27*, 5524.

62. Dallmeyer, I.; Chowdhury, S.; Kadla, J. F. *Biomacromolecules* **2013**, *14*, 2354.

63. Dai, Z.; Shi, X.; Liu, H.; Li, H.; Han, Y.; Zhou, J. *RSC Adv.* **2018**, *8*, 1218.

64. Zhang, R.; Du, Q.; Wang, L.; Zheng, Z.; Guo, L.; Zhang, X.; Yang, X.; Yu, H. *Green Chem.* **2019**, *21*, 4981.
65. Torres-Canas, F.; Bentaleb, A.; Föllmer, M.; Roman, J.; Neri, W.; Ly, I.; Derré, A.; Poulin, P. *Carbon N. Y.* **2020**, *163*, 120.
66. Ferrari, A. C.; Robertson, J. *Phys. Rev. B* **2000**, *61*, 14095.
67. Dallmeyer, I.; Lin, L. T.; Li, Y.; Ko, F.; Kadla, J. F. *Macromol. Mater. Eng.* **2014**, *299*, 540.
68. Ou, Y.; González, C.; Vilatela, J. J. *Compos. Part B Eng.* **2020**, *201*.
69. Dhakate, S. R.; Chaudhary, A.; Gupta, A.; Pathak, A. K.; Singh, B. P.; Subhedar, K. M.; Yokozeki, T. *RSC Adv.* **2016**, *6*, 36715.
70. Sadrjahani, M.; Gharehaghaji, A. A.; Javanbakht, M. *Polym. Eng. Sci.* **2017**, *57*, 789.
71. Chan, S.; Jankovic, J.; Susac, D.; Saha, M. S.; Tam, M.; Yang, H.; Ko, F. *J. Mater. Sci.* **2018**, *53*, 11633.